energies

MDPI

Article

A Study of Thermoelectric Generation Coupled with Methanol Steam Reforming for Hydrogen Production

Guoqiang Wang [1,2], Feng Wang [1,2,3,*] and Delun Guan [1,2]

[1] School of Energy and Power Engineering, Chongqing University, Chongqing 400044, China
[2] Key Laboratory of Low-Grade Energy Utilization Technologies and Systems, Chongqing University, Ministry of Education, Chongqing 400044, China
[3] Department of Nuclear Engineering and Technology, Chongqing University, Chongqing 400044, China
* Correspondence: wangfeng@cqu.edu.cn; Tel.: +86-13618203569

Abstract: Waste heat recovery was considered as a promising candidate for energy conservation and emission reduction. Methanol steam reforming was considered to be an effective means for hydrogen production because of its advantages. In this work, a micro reactor was constructed and thermoelectric generation coupled with hydrogen production from methanol steam reforming was innovatively used to recycle waste heat, which was simulated by hot air from a hot air gun. The waste heat was converted into electricity and hydrogen at the same time. The characteristic of thermoelectric generation coupled with methanol steam reforming was investigated. It was experimentally verified that both the hydrogen production rate and methanol conversion increased with the increasing inlet temperature, but thermal efficiency increased firstly and then decreased with the increasing temperature. The methanol steam reforming could effectively maintain cold side temperature distribution of thermoelectric generation. In the case of the thermoelectric module (1), the highest temperature difference of 37 °C was determined and the maximum open circuit voltage of 2 V was observed. The highest methanol conversion of 64.26% was achieved at a space velocity of 0.98 h^{-1} when the temperature was 543 K, comprehensively considering the CO content and thermal efficiency.

Keywords: energy conversion; hydrogen energy; methanol steam reforming; thermal management and control; waste heat recovery

Citation: Wang, G.; Wang, F.; Guan, D. A Study of Thermoelectric Generation Coupled with Methanol Steam Reforming for Hydrogen Production. *Energies* **2022**, *15*, 8155. https://doi.org/10.3390/en15218155

Academic Editor: Eugenio Meloni

Received: 24 September 2022
Accepted: 28 October 2022
Published: 1 November 2022

1. Introduction

Low-grade surplus heat or waste heat with a temperature of higher than 200 °C widely exists in industrial furnaces, engines, and the metallurgical industry. Waste heat energy takes up about 17–67% of the total energy consumption, so waste heat recovery is vital for energy conservation and emission reduction [1,2]. A study found a thermal efficiency improvement of 6% in a Rankine cycle system powered by exhaust gas [3]. The recovery of engine waste heat by ORC was evaluated to result in a 5–11.3% reduction in its specific fuel consumption and in an increase of about 5% in the engines' thermal efficiency [4]. The recovery of engine waste heat by organic Rankine cycle could increase by 5% of the engines' thermal efficiency, resulting in a 5–11.3% reduction in its specific fuel consumption [5].

At present, many studies have focused on waste heat recovery by thermoelectric power generation [6–8]. L Bao et al. proposed a novel thermoelectric generator system based on liquid metal that serves to collect and transfer waste heat [9]. The open-circuit voltage reached 34.7 V when the temperature of the waste heat source was 195.9 °C and the temperature difference between the plates of cooling-water and liquid metal heating plate was about 100 °C. A study investigated the thermoelectric generation performances heated by the wasted flue gas heat [10]. These characteristics were also affected by the thermal contact resistance from the study of Shixue Wang et al. [11]. They found that the

temperature gap of the thermoelectric module and the output power increased when an interface material was utilized for the contact surface at a given temperature difference between the cold and hot sources. Fankai Meng et al. reported a method to recover waste heat using thermoelectric power generation technology [12]. They determined that the design of heat recuperation is vital for the characteristics of air-cooling thermoelectric power generation equipment.

As compared with other hydrocarbon fuels, a small amount of CO could be detected in the products in methanol steam reforming (MSR) because of the relatively low conversion temperature. Methanol steam reforming (MSR) is an endothermic catalytic reaction and requires a lot of external heat for the reactant vaporization, super heating, and reaction process [13,14]. In an MSR reactor, thermal resistance results in the temperature difference between its heating channel and reforming channel [15]. For the reforming reaction, when the heat sources are different (such as industrial waste gas, engine waste heat, high-temperature helium gas-cooled reactor heat source, catalytic combustion heat, electric heating source, and so on), the characteristics of reactor temperature and temperature difference will be very distinct [16,17]. MSR reactors have increasingly been recognized in recent years as a novel tool for waste heat recovery [2,18]. The novel MSR reactors offer a higher heat transfer rate because of their high surface-to-volume ratio and short conduction paths [19]. However, there were also several difficulties and challenges. When using micro-reactors in heterogeneously catalyzed gasphase reactions, random packing would result in a high pressure drop [20]. The temperature difference due to the heat transfer process between the heating channel and reforming channel can be used to generate electricity through thermoelectric generation modules. This measure can not only can improve energy utilization efficiency, but also provide electrical energy by the thermoelectric module when the reforming reaction begins at room temperature [21].

In this study, an innovative heat recuperation design was carried out using the endothermic MSR to remove the heat from the thermoelectric module cold side. Waste heat simulated by hot air was used as the heat source of the thermoelectric module on the hot side. The characteristic of thermoelectric generation coupled with hydrogen production from MSR was investigated experimentally.

2. Experimental

2.1. Reactor Design

A stainless steel microreactor was designed and fabricated, as shown in Figure 1. It included a reforming channel, thermoelectric module, and heating channel. Along the reactants' flowing direction, five thermoelectric generation modules lay between the reforming and heating channels, which were numbered (1) to (5) from the inlet to the outlet of the reactor successively. The MSR took place in the chamber with a length, width, and height of 200 mm, 40 mm, and 10 mm, respectively. The commercial catalyst of $CuO/ZnO/Al_2O_3$ (CB-7) was used with a weigh of 21 g, which was diluted by quartz sand. The corresponding size of thermoelectric power generation module was 40 mm × 40 mm × 5 mm. The reactor was made of 304 stainless. As MSR is endothermic, intense inlet temperature changes occur at the inlet of the reforming channel. Therefore, temperature-measuring points at the reforming channel inlet were specially designed for three rows. In addition, centre points of hot and cold sides of each thermoelectric generation modules were measured.

2.2. Experiment System and Procedure

The experiment system of MSR coupled with thermoelectric generation is shown in Figure 2. Methanol used in the experiment was analytically pure with a mass fraction greater than 99.5%. The water was deionized water prepared by ultra-pure water machine. Experiments were carried out at atmospheric pressure. The methanol and water mixture solution was sent to the reforming channel through a peristaltic pump. Studies showed that a water/methanol ratio of 1.3 is appropriate for a copper-based catalyst in MSR, so a water/methanol ratio of 1.3 was selected [22]. Samples were collected after the reaction tem-

perature was steady. Unreacted water and methanol vapour were cooled in an ice bath and then separated using a gas–liquid separator. The dry gas flow rate was measured by a soap foam flow meter. The composition of gas and liquid was analyzed by gas a chromatography (GC3000) equipped with Porapak Q and TDX-01 columns. Helium was used as the carrier gas for the gas chromatograph. Before the reaction, N_2 was passed through the system to exclude the air, then H_2-N_2 (3% Vol.) was used for the catalyst temperature-programmed reduction and activation until the outlet H_2 composition remained unchanged, indicating the ending of the reduction process.

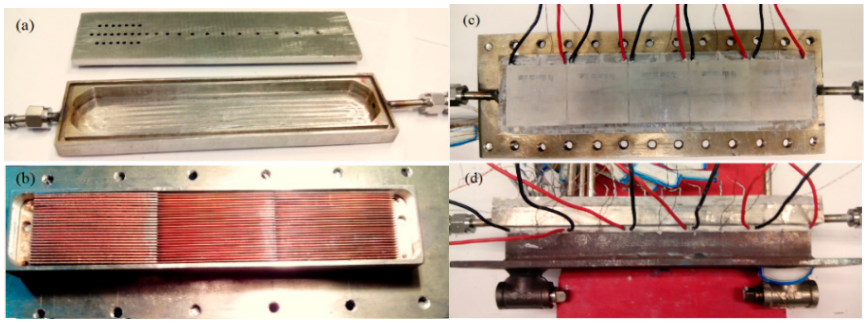

Figure 1. Methanol steam reforming reactor coupled with thermoelectric power generation modules: (**a**) reforming channel; (**b**) heating channel; (**c**) thermoelectric modules arrangement; and (**d**) reactor assembling.

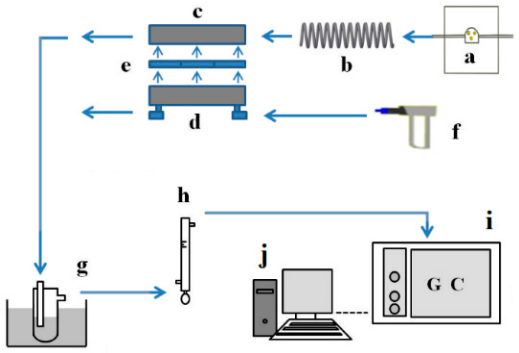

Figure 2. System of methanol steam reforming coupled with the thermoelectric module: (a) peristaltic pump, (b) vapourization and superheating heater, (c) reforming channel, (d) heating channel, (e) thermoelectric module, (f) hot air gun, (g) ice trap and gas liquid separator, (h) soap foam flow meter, (i) chromatography, and (j) workstation and computer.

3. Results and Discussion

3.1. Temperature Rising Characterization of the Reformer

A hot air gun was used to provide the hot air, which simulated the waste heat. The voltage of the hot air gun, which was used to heat the reactor, was 135 V. The mass flow rate of hot air at the outlet was 0.04 g/s; this flow rate was regarded as the inlet flow rate of hot air from the hot air gun. The initial entrance air temperature of the hot air gun was room temperature and the final stable temperature was kept at about 490 °C. The space velocity of methanol and water reactant at the reactor reforming side was 1.53 h^{-1}. The variation in the reactor heating side inlet temperature ($T_{heater\text{-}in}$), the temperature at the reactor reforming side inlet (L = 5 mm) (T_{SR}), the temperature difference between the hot and cold sides of the thermoelectric module (1) (ΔT_{TE}), and its open-circuit voltage ($V_{TE\text{-}open}$) were studied; the results are shown in Figure 3.

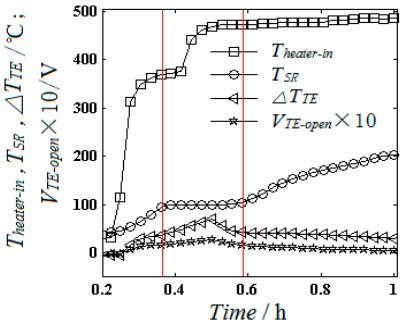

Figure 3. Variation in $T_{heater-in}$, T_{SR}, ΔT_{TE}, and $V_{TE-open}$ with time.

As can be seen from Figure 3, $T_{heater-in}$ rose rapidly at the initial heating stage (0–0.3 h) and then began to be stabilized at about 380 °C. Influenced by $T_{heater-in}$, T_{SR} also gradually increased to 100 °C, which was the highest vapourization temperature of methanol water fluid reactants, and then remained constant. However, there was a 0.15 h time delay of T_{SR} compared with the temperature rising time of $T_{heater-in}$. At the time of 0.43 h, when adjusting the heating voltage to 140 V, $T_{heater-in}$ quickly rose to 490 °C and then remain unchanged. However, T_{SR} still remained at 100 °C from the time of 0.36 h to 0.59 h, as thermal resistance exists between the heating channel and reforming channel. Latent heat for reactant vaporization also needs to absorb lots of heat from the heating channel, which also delayed the temperature rise in the steam reforming channel. As for the temperature difference of module (1) between its hot and cold sides, ΔT_{TE} rose firstly to a maximum value of 70 °C and then decreased gradually. The main reason was that, in the initial stage, at the steam reforming channel inlet, where the thermoelectric module (1) is located, the temperature on its cold side remained constant at 100 °C; however, its hot side temperature increased gradually as a result of the rising of $T_{heater-in}$. Therefore, ΔT_{TE} increased firstly. After the temperature of the heating channel stayed constant, due to heat resistance between the module (1) cold side and steam reforming channel, the temperature on the module (1) cold side continually rose, so ΔT_{TE} began to decrease gradually. Furthermore, as time progressed, reactant vaporization in the steam reforming channel became stable, and ΔT_{TE} continually decreased after the temperature in the steam reforming channel exceeded 100 °C. Therefore, ΔT_{TE} presents a variation of increasing firstly and then decreasing gradually, as shown in Figure 3. Open circuit voltage variation of module (1) was the same as that of temperature difference ΔT_{TE}, although its variation amplitude was smaller. The maximum $V_{TE-open}$ reached 2 V.

At the condition of reactant space velocity of 1.53 h^{-1}, the air mass flow rate on the heating side of 0.04 g/s, $T_{heater-in}$ of 490 °C, and variations in temperature with time along the reforming channel between 0.3 and 0.9 h are shown in Figure 4. The results showed that temperatures at all measurement points within the reforming passage gradually increased as time progressed. Until reaching a time period of about 0.4–0.6 h, all measurement points' temperatures reached the water vaporization temperature of 100 °C successively. The closer to the reforming channel inlet side of the measurement points, the earlier the time at which the vaporization temperature reached 100 °C, and vice versa. The temperature of the last measurement points in the reforming channel reached the gasification temperature at a time of 0.5 h, while it had a delay of 0.1 h compared with the first point in the reforming channel. After 0.6 h, the temperature of all measurement points in the reforming channel exceeded the water vaporization temperature, and then they began to increase gradually. Besides, the processes of all measurement points' temperature increases were almost synchronous. It could also be seen from the figure that, except for the gasification process, the reforming channel temperature difference between its inlet and outlet was about 30 °C, mainly because of the endothermic nature of the methanol steam reforming reaction.

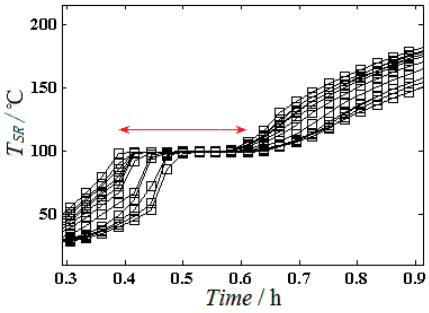

Figure 4. Temperature variation at different measurement points in the reforming channel between 0.3 and 0.9 h.

3.2. Characteristic of Temperature Difference between the Hot and Cold Sides of the Thermoelectric Module

Furthermore, the variation in temperature difference between the thermoelectric modules' (1)–(5) hot and cold sides with time during 0–14 h was investigated. In this case, the voltage of the hot air gun was fixed at 135 V; the flow rate at the heating side was 0.04 g/s. Because the hot air gun voltage remained constant, the inlet gas temperature at the heating side was only influenced by the voltage of the hot air gun; therefore, the inlet temperature at the heating side rose rapidly from about 380 °C to about 480 °C and then maintained constant. Methanol and water space velocity (*WHSV*) at the reforming side increased from 0.30 h^{-1} to 3.80 h^{-1}. The results are shown in Figure 5.

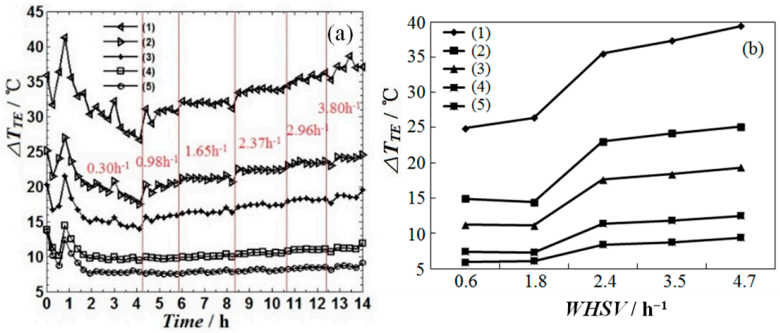

Figure 5. Variation in temperature difference of the thermoelectric modules with time (**a**) and space velocity (**b**).

As can be seen from Figure 5a, in the time of 2 h after the reformer began to run, the variation in ΔT_{TE} with time is drastic, especially for that of modules (1)–(3), which were in the front section of the reformer. It presented a decrease and then an increase, and again a variation in the decrease. It could be inferred from the variation that, at the same heating condition, the reforming channel experienced the reactant vapourization, superheating, and endothermic reaction process. After 2 h, ΔT_{TE} of the thermoelectric modules began to stabilize. Furthermore, it can also be seen that ΔT_{TE} decreased from module (1) to module (5). The reason is that, from module (1) to (5), the reactant of methanol and water was gradually consumed by the steam reforming reaction. The heat required for this endothermic reaction decreased gradually along the reforming channel. Thus, the temperature in the steam reforming channel increased gradually, which finally resulted in the decrease in ΔT_{TE}. From Figure 5a,b, it could also be concluded that ΔT_{TE} increases with the increase in *WHSV*. This is because, as WHSV increases, the flow rate of methanol and water reactants in the steam reforming channel increases, and the absolute reactant conversion rate increases under the same heating conditions, although the methanol conversion rate may decrease. This leads to the increase in heat absorbed by the methanol steam reforming reaction. Therefore, the temperature on the thermoelectric module cold side decreased and, consequently, ΔT_{TE} increased.

The results from Figure 5a,b also show that the effect of *WHSV* decreased gradually from thermoelectric module (1) to (5). It is also suggested that the endothermic reaction of methanol steam reforming was more intense near the inlet of the reactor than that at the outlet. At position 3/5 of the reactor along the reactant flow direction, methanol was mostly converted. Therefore, the contribution of heat removal by the methanol steam reforming reaction is weak. The temperature difference of thermoelectric module (1) was the highest owing to the strongest endothermic reaction at the reforming channel inlet. The rate of heat supplied from the heating channel may be insufficient at the inlet for methanol steam reforming, which leads to the highest temperature difference between the thermoelectric hot and cold side. It could be inferred from the above analysis that the key factor for maintaining the thermoelectric module cold side and hot side temperature difference lies in the heat-removing rate on its cold side. The adoption of liquid phase-change material such as water and methanol is one of the efficient ways to removed its heat on the cold side. It was even more optimal to adopt an endothermic reaction such as methanol steam reforming for heat recuperation on its cold side for large heat removal rates. Not only was the grade of the fuel improved by means of steam-reform heated by waste heat, but also electricity was generated by this method.

In addition, the space velocity was fixed at 0.98 h^{-1} on the reforming side and the variation in temperature difference of the thermoelectric modules with time was studied. The mass flow rate of the heating gas was 0.04 g/s. The voltage of the hot air gun was set to 115 V, 125 V, 130 V, 135 V, and 140 V step by step. As could be seen from Figure 6, the temperature difference of ΔT_{TE} increased quickly at first when the hot air gun voltage stepped up and then decreased gradually. When the voltage of the hot air gun increased, the heat generated by the hot air gun increased, which led to the increase in temperature in the heating channel. Consequently, the temperature on the thermoelectric module hot side increased. The temperature at the reforming channel inlet also increased from 190 °C to 275 °C step by step, as shown in Figure 6. However, it took time for the heat to transfer to the thermoelectric module cold side, so the temperature difference of ΔT_{TE} increased at first. After the transient heat transfer process, the thermoelectric module cold side temperature began to increase, leading to the decrease in ΔT_{TE}. It could also be seen from Figure 6 that the variation in ΔT_{TE} was severe in the first two hours, which may be caused by the reaction and transport transient in the start time. Then, it increased a little and decreased gradually. From the results, it can also be inferred that the values of ΔT_{TE} were larger for the thermoelectric module located at the front part of the reformer than that located at the rear of the reformer. Furthermore, there was a time delay of the highest temperature difference for thermoelectric modules (1) to (5). It became more and more obvious from thermoelectric modules (1) to (5), which illustrated that more time is needed for the heat balance from the reactor inlet to reactor outlet.

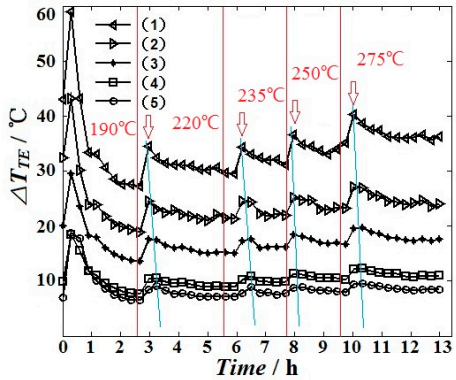

Figure 6. Variation in temperature difference of thermoelectric modules with time.

At the condition of reforming channel inlet temperature of 235 °C, the temperatures of thermoelectric modules' (1) to (5) hot and cold sides along the flow direction are shown in

Figure 7. Both the hot side temperature and cold side temperature of the thermoelectric module decreased along the reactant flow direction. The hot side temperature decreased from 590 °C linearly to 530 °C and the temperature on the cold side decreased from 560 °C to 525 °C. Therefore, the corresponding thermoelectric temperature difference ΔT_{TE} decreased from 30 °C to 5 °C. Furthermore, from Figure 7, it could be seen that the temperature decreasing on the thermoelectric module (1) cold side was more severe than that on the other modules, which also states that, at the reforming channel inlet, with methanol steam, the reforming reaction was the strongest.

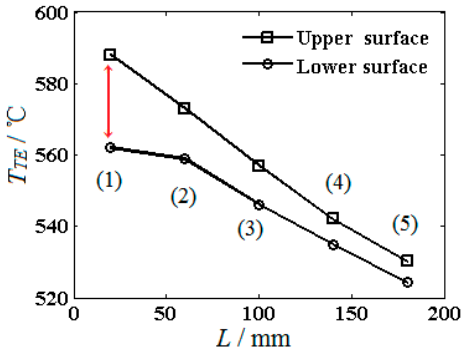

Figure 7. Thermoelectric modules' (1) to (5) hot and cold side temperature distribution along the flow direction.

3.3. Performance of the Reformer for Hydrogen Production

Three equations can describe the three main reactions for this combination of reactants and products [23].

$$CH_3OH \rightarrow CO + 2H_2 \qquad \Delta H^o_{298} = +92.0\ \mathrm{KJ/mol} \tag{1}$$

$$CO + H_2O \leftrightarrow CO_2 + H_2 \qquad \Delta H^o_{298} = -41.1\ \mathrm{KJ/mol} \tag{2}$$

Equation (1) represents the methanol decomposition and Equation (2) represents the water gas shift reaction. The methanol conversion X_{MeOH}, H_2 production rate V_{H2}, and space velocity $WHSV$ can be calculated by the following equation:

$$X_{MeOH} = \frac{F(y_{co} + y_{co2})}{22.4 \times v_{MeOH,in}} \times 100\% \tag{3}$$

$$V_{H2} = F \times y_{H2} \tag{4}$$

$$WHSV = \frac{32 \times v_{MeOH,in}}{M} \tag{5}$$

where F is flow rate of effluent gas, y is the volumetric fraction, $v_{MeOH,in}$ is the molar flow rate of methanol fed into the reactor, and M is the mass of catalyst [24]. Reformer performance was important for the optimum parameters' selection of the thermoelectric module. At a space velocity of 0.98 h^{-1}, variations in the hydrogen production rate (Y_{H2}), methanol conversion (X_{CH3OH}), temperature difference between module (1) hot and cold sides (ΔT), and heating channel thermal efficiency (η_{heater}) with reforming channel inlet temperature were studied. The results are shown in Figure 8. Here, the heating channel thermal efficiency (η_{heater}) was defined as the ratio of MSR heat absorption at the reforming side and the heat release at the heating channel.

As shown in Figure 8, at a relatively lower temperature ($T_{SR\text{-}in}$ < 235 °C), Y_{H2}, X_{CH3OH}, and ΔT of module (1), as well as η_{heater}, were all increased rapidly with the increase in the reforming channel inlet temperature. When the reforming channel inlet temperature exceeded 235 °C, the rate of increase in the methanol conversion and hydrogen production rates dropped. In this case, continued improvement in the hot air gun heating voltage

would not increase the amount of reaction, and excess heat may accumulate at the module hot side and temperature differences of module (1) continued to increase. Finally, it reached as high as 37 °C. As the increment of the methanol conversion rate was less than that of the heating power, heater efficiency decreased with increase in temperature. Thus, when the reactor reforming channel inlet temperature reached 235 °C, the hydrogen production rate and methanol conversion reached the optimum value, and heater efficiency also reached its maximum value. Upon continuing to increase the temperature, the increase in the methanol conversion and hydrogen production rate was not obvious, but led to a lower heater efficiency. The experimental methanol conversion X_{CH3OH} was lower than the methanol conversion $X_{CH3OH\text{-}TE}$ of thermodynamic equilibrium data [25]. The MSR reactor suffered from severe limitations of mass and heat transfer. These disadvantages led to thermal stresses, which significantly affected the catalyst performance characteristics. Furthermore, because of the severe transfer resistance, the MSR reformers were limited to a low effectiveness factor of the catalyst. Although the temperature difference between thermoelectric module (1) hot and cold side still increased, the problem of increased CO content caused by a higher temperature needs to be considered because it is a kind of poison gas for PEMFC. In general, the reactor reforming channel inlet temperature of 235 °C is an optimum operating parameter in this condition. In addition, as the heat of unreacted methanol and water, heat of products, and thermoelectric power output were not included in the heater thermal efficiency calculation, the actual thermal efficiency of the heater should be higher than that obtained in this experiment.

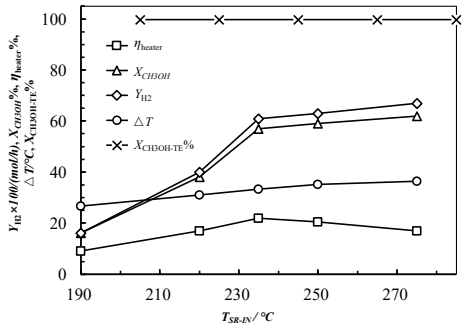

Figure 8. Variation in Y_{H2}, X_{CH3OH}, and ΔT of module (1), as well as η_{heater} and $X_{CH3OH\text{-}TE}$%, with the reforming channel inlet temperature.

At the condition of reforming channel inlet temperature of 235 °C, variation in Y_{H2}, X_{CH3OH}, and ΔT of module (1), as well as η_{heater}, with reforming channel inlet $WHSV$ was investigated. The results are shown in Figure 9. As could be seen from Figure 9, Y_{H2}, ΔT, and η_{heater} all increased with the space velocity, while X_{CH3OH} decreased with the increase in space velocity. As for Y_{H2} and η_{heater}, they presented a similar variation with the increase in space velocity. They both increased linearly when space velocity was less than 3 h^{-1}, then the increasing rate slowed down when space velocity was higher than 3 h^{-1}. The resident time of the reactant decreased with a higher WHSV, resulting in the reforming reaction not being completed in the catalyst bed. This is why the methanol conversion decreased with an increasing WHSV. Therefore, methanol conversion, hydrogen production rate, heater efficiency, and output power of thermoelectric module should be taken into account in the selection of the optimum operating parameters. From the above results, when the reactant space velocity remains at 3.0 h^{-1}, methanol conversion, hydrogen production rate, temperature difference of module (1), and heater efficiency were all relatively high. A further increase in space velocity cannot increase the reactor performance significantly, so this space velocity was one of the optimum operating parameter at this temperature.

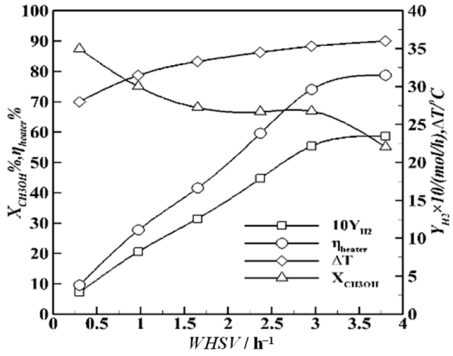

Figure 9. Variation in Y_{H2}, X_{CH3OH}, and ΔT of module (1), as well as η_{heater}, with reforming channel inlet *WHSV*.

Furthermore, as shown in Figure 10, the variation of thermoelectric module (1) hot and cold side temperature difference ΔTTE with different space velocity was also studied at the condition of hot air gun voltage of 135 V. The reactants used in the reforming side are methanol water solution and water only. As could be seen in Figure 10, for both the water and methanol water solution, ΔTTE increased with the increase in space velocity. When space velocity was lower, the methanol water solution has a larger ΔTTE. This indicated that a strong endothermic methanol steam reforming reaction has a larger contribution to the heat removal on thermoelectric module cold side. With the increase in space velocity, values of ΔTTE for both water and methanol water solution increased and approached being equal, which indicated that the heat absorbed by methanol steam reforming reaction system and water vapourization is almost the same. Moreover, methanol conversion may be completed at that range of WHSV. Then, with the further increase in WHSV, the methanol flow rate in the reforming channel increased and the amount of methanol involved in the reaction increased. Therefore, the heat absorbed by steam reforming increased and the thermoelectric module cold side temperature decreased. Finally, ΔTTE still further increased for the methanol water solution compared with that of water only.

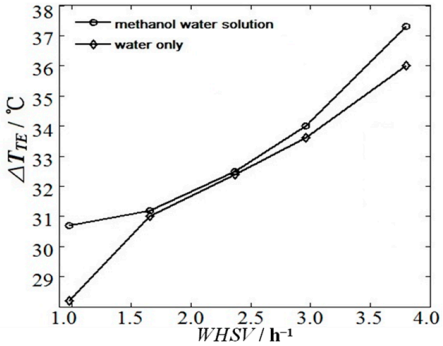

Figure 10. Variation in ΔT_{TE} with space velocity at different reactants in the reforming channel.

4. Conclusions

An innovative heat recuperation device design was carried out using the endothermic catalytic reaction to remove the heat from the thermoelectric module cold side. The characteristic of MSR for hydrogen production coupling thermoelectric generation was investigated through an experiment. The endothermic methanol steam reforming reaction is an effective method for heat removal at the thermoelectric module cold side. Methanol conversion, hydrogen production rate at reforming channel, and the temperature difference of thermoelectric module increased with the increase in the reforming channel inlet temperature. In the temperature rising process, the reactant in the reforming channel went through the stages of liquid fuel vapourization, superheating, and reaction. In the vapourization process, the temperature difference between the thermoelectric module hot and cold sides

achieved the highest level and then decreased gradually. Along the flowing direction, there was a time delay of reactant vapourization in the reforming channel at its outlet local area. The endothermic steam reforming reaction and increase in heating temperature led to stronger temperature difference fluctuations at the beginning. The maximum open circuit voltage of thermoelectric module (1) was 2 V. The temperature and temperature difference of thermoelectric modules gradually decreased along the flow direction. An increase in space velocity had a greater impact on the temperature difference in the front section of reformer, while it was non-significant on that in the back of the reformer. Nevertheless, the influence of temperature was smaller than that of space velocity. Comprehensively considered with CO content and thermal efficiency, the highest conversion of 64.26% was achieved at a space velocity of 0.98 h^{-1} when the temperature was 543 K.

Author Contributions: Conceptualization, F.W. and G.W.; formal analysis, G.W. and F.W.; resources, G.W. and F.W.; writing—original draft preparation, G.W. and D.G.; writing—review and editing, F.W., G.W. and D.G.; supervision, F.W.; project administration, F.W.; funding acquisition, F.W. and G.W. All authors have read and agreed to the published version of the manuscript.

Funding: This research was funded by Chongqing technology innovation and application demonstration project (CSTC2018JSZX-CYZDX0100) and National Key R&D Program of the People's Republic of China (2018YFB0104502).

Institutional Review Board Statement: Not applicable for studies not involving humans or animals.

Informed Consent Statement: Not applicable.

Data Availability Statement: Not applicable.

Conflicts of Interest: The authors declare no conflict of interest.

References

1. Ganguly, A.; Sengupta, S.; Pramanik, S. Waste heat recovery using Tesla turbines in Rankine cycle power plants: Thermofluid dynamic characterization, performance assessment and exergy analysis. *Appl. Therm. Eng. Des. Processes Equip. Econ.* **2022**, *12*, 207–219. [CrossRef]
2. Bakanos, P.I.; Katsifarakis, K.L. Optimizing Current and Future Hydroelectric Energy Production and Water Uses of the Complex Multi-Reservoir System in the Aliakmon River. *Energies* **2020**, *13*, 6499. [CrossRef]
3. Kang, H.S.; Kim, M.H.; Shin, Y.H. Thermodynamic Modeling and Performance Analysis of a Combined Power Generation System Based on HT-PEMFC and ORC. *Energies* **2020**, *23*, 6163. [CrossRef]
4. Kumar, C.; Rana, K.B.; Tripathi, B. Effect of diesel-methanol-nitromethane blends combustion on VCR stationary CI engine performance and exhaust emissions. *Environ. Sci. Pollut. Res.* **2019**, *26*, 6517–6531. [CrossRef]
5. Jung, G.; Chan, S.; Lai, C. Innovative membrane electrode assembly (MEA) fabrication for proton exchange membrane water electrolysis. *Energies* **2019**, *12*, 4218. [CrossRef]
6. Deb, P.; Debnath, P.; Denis, A.F.; Lepcha, O.T. Variability of soil physicochemical properties at different agroecological zones of Himalayan region: Sikkim, India. *Environ. Dev. Sustain.* **2019**, *21*, 2321–2339. [CrossRef]
7. Andrade, T.S.; Papagiannis, I.; Dracopoulos, V. Visible-light activated titania and its application to photoelectrocatalytic hydrogen peroxide. *Materials* **2019**, *12*, 4238. [CrossRef]
8. Chen, T.Z.; Ge, Y.L.; Liu, Y.C.; He, H. VOCs Emission from Motor Vehicles in China and Its Impact on the Atmospheric Environment. *Environ. Sci.* **2018**, *39*, 478–492.
9. Bao, L.; Han, Y.; Zhang, Y.; Meng, Q. Thermoelectric generation technology and design of thermoelectric generation system for industrial waste heat recovery. *Ordnance Mater. Sci. Eng.* **2015**, *10*, 132–146.
10. Yamamoto, K.; Iguchi, R.; Miura, A.; Zhou, W.; Sakuraba, Y.; Miura, Y.; Uchida, K.I. Phenomenological analysis of transverse thermoelectric generation and cooling performance in magnetic/thermoelectric hybrid systems. *J. Appl. Phys.* **2021**, *15*, 257–268. [CrossRef]
11. Wang, S.; Xie, T.; Xie, H. Experimental study of the effects of the thermal contact resistance on the performance of thermoelectric generator. *Appl. Therm. Eng. Des. Processes Equip. Econ.* **2018**, *130*, 847–853. [CrossRef]
12. Meng, F.; Chen, L.; Xie, Z.; Ge, Y. Thermoelectric generator with air-cooling heat recovery device from wastewater. *Therm. Sci. Eng. Prog.* **2017**, *4*, 106–117. [CrossRef]
13. Wang, H.; Yang, R.; Wang, B.; Wei, Z.; Kong, H.; Lu, X.; Jin, J. Thermodynamic performance of solar-driven methanol steam reforming system for carbon capture and high-purity hydrogen production. *Appl. Therm. Eng. Des. Processes Equip. Econ.* **2022**, *12*, 209. [CrossRef]

14. Huang, H.K.; Chih, Y.K.; Chen, W.H.; Hsu, C.Y.; Lin, K.J.; Lin, H.P.; Hsu, C.H. Synthesis and regeneration of mesoporous Ni–Cu/Al_2O_4 catalyst in sub-kilogram-scale for methanol steam reforming reaction. *Int. J. Hydrog. Energy* **2021**, *4*, 253–267.
15. Matus, E.; Sukhova, O.; Ismagilov, I.; Kerzhentsev, M.; Stonkus, O.; Ismagilov, Z. Hydrogen Production through Autothermal Reforming of Ethanol: Enhancement of Ni Catalyst Performance via Promotion. *Energies* **2021**, *14*, 5176. [CrossRef]
16. Ali Cherif, R.N. Numerical analysis on autothermal steam methane reforming: Effects of catalysts arrangement and metal foam insertion. *Int. J. Hydrog. Energy* **2019**, *44*, 22455–22466. [CrossRef]
17. Pashchenko, D. Liquid organic hydrogen carriers (LOHCs) in the thermochemical waste heat recuperation systems:the energy and mass balances. *Int. J. Hydrog. Energy* **2022**, *47*, 28721–28729. [CrossRef]
18. Matus, E.V.; Ismagilov, I.Z.; Yashnik, S.A.; Ushakov, V.A.; Prosvirin, I.P.; Kerzhentsev, M.A.; Ismagilov, Z.R. Hydrogen production through autothermal reforming of CH4: Efficiency and action mode of noble (M $\frac{1}{4}$ Pt, Pd) and non-noble (M $\frac{1}{4}$ Re, Mo, Sn) metal additives in the composition of Ni-M/$Ce_{0.5}Zr_{0.5}O_2/Al_2O_3$ catalysts. *Int. J. Hydrog. Energy* **2020**, *45*, 33352–33369. [CrossRef]
19. Yuan, T.; Duan, Q.; Chen, X. Coordinated control of a wind-methanol-fuel cell system with hydrogen storage. *Energies* **2017**, *12*, 2053. [CrossRef]
20. Feng, W.; Cao, Y.; Wang, G. Thermoelectric generation coupling methanol steam reforming characteristic in microreactor. *Energy* **2014**, *80*, 642–653.
21. Luo, D.; Wang, R.; Yu, W.; Zhou, W. Parametric study of asymmetric thermoelectric devices for power generation. *Int. J. Energy Res.* **2020**, *8*, 44. [CrossRef]
22. Wang, G.; Wang, F.; Chen, B. Performance Study on Methanol Steam Reforming Rib Micro-Reactor with Waste Heat Recovery. *Energies* **2020**, *13*, 1564. [CrossRef]
23. Yu, D.; Kim, B.; Ji, H.; Yu, S. Sensitivity Analysis of High-Pressure Methanol—Steam Reformer Using the Condensation Enthalpy of Water Vapor. *Energies* **2022**, *15*, 3832. [CrossRef]
24. Jung, S.K.; Cha, W.S.; Park, Y.I.; Kim, S.H.; Choi, J. Conceptual Design Development of a Fuel-Reforming System for Fuel Cells in Underwater Vehicles. *Energies* **2020**, *13*, 2000. [CrossRef]
25. Chen, M.; Sun, G.; Wang, Y.; Liang, D.; Li, C.; Wang, J.; Liu, Q. Steam reforming of methanol for hydrogen production over attapulgite-based zeolite-supported Cu-Zr catalyst. *Fuel J. Fuel Sci.* **2022**, *15*, 314. [CrossRef]